ACS APPLIED MATERIALS & INTERFACES

Research Article

www.acsami.org

"Mixed-charge Self-Assembled Monolayers" as A Facile Method to Design pH-induced Aggregation of Large Gold Nanoparticles for Near-Infrared Photothermal Cancer Therapy

Huan Li,† Xiangsheng Liu,† Nan Huang, Kefeng Ren, Qiao Jin, and Jian Ji*

MOE Key Laboratory of Macromolecular Synthesis and Functionalization, Department of Polymer Science and Engineering, Zhejiang University, Hangzhou 310027, China

Supporting Information

ABSTRACT: The acidic microenvironment of tumor tissues has proven to be one of the major differences from other normal tissues. The near-infrared (NIR) light irradiation of aggregated gold nanoparticles in a tumor acidic pH-induced manner could then provide an effect approach to treat solid tumors with the advantage of minimizing the undesired damage to normal tissues. Although it is well-known the aggregation of larger nanoparticles will result in a better NIR photothermal effect, the preparation of pH-sensitive gold nanoparticles in large sizes remains a big challenge because of their worse dispersive stability. In this paper, we introduce a facile way to endow large gold nanoparticles with tunable pH-aggregation behaviors by modifying the nanoparticle surface with mixed-charge self-assembly monolayers compromising positively and negatively charged thiol ligands. Four different size nanoparticles were used to study the general principle of tailoring the pH-induced aggregation behaviors of mixed-charge gold nanoparticles (MC-GNPs) by adjusting the surface ligand composition. With proper surface ligand composition, the MC-GNPs in four different sizes that all exhibited aggregation at tumor acidic pH were obtained. The biggest MC-GNPs showed the most encouraging aggregation-enhanced photothermal efficacy in vitro when they formed aggregates. The mixed-charge self-assembled monolayers were then proved as a facile method to design pH-induced aggregation of large gold nanoparticles for better NIR photothermal cancer therapy.

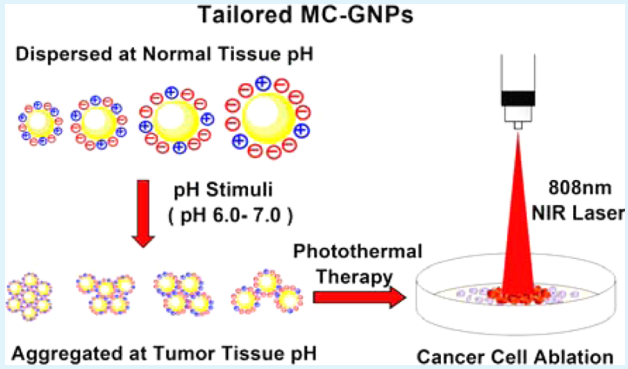

KEYWORDS: *mixed-charge gold nanoparticles, pH-induced aggregation, size effect, near-infrared (NIR) photothermal therapy*

1. INTRODUCTION

Photothermal therapy collaborating with the near-infrared (NIR) light (650−900 nm) irradiation has been considered as an attractive way to treat solid tumors with the advantages of minimally invasiveness, fast recovery and fewer complications.[1−3] Certain photosensitizers are needed at the solid tumor site to convert the NIR light into available heat, by which the thermalsensitive tumor cells can be effectively killed.[4] Several gold nanomaterials, such as gold nanorods,[5−7] nanocages,[8−10] nanoshells[11,12] and nanohexapods[13] have been developed for the NIR photothermal cancer therapy utilizing the plasmon−enabled photothermal conversion properties.[14] Though encouraging photothermal efficacy has been realized by those gold photosentisizers both in vitro[15,16] and in vivo,[17−19] further application is greatly limited by their complicated structure and unclear biological toxicity.[20,21] Compared with the nanomaterials mentioned above, spherical gold nanoparticles are well-developed nanomaterials that are nontoxic, simple in structure and easy to prepare,[19] but they have been less favored in the NIR photothermal therapy for their inefficient absorption of the NIR light.[22] What's interesting is that when gold nanospheres aggregate, there is a red-shift in the light absorption spectrum, which dramatically enhances the light absorbance in the NIR region, opening up new opportunities for nanospheres to be utilized as photosensitizers in the NIR photothermal therapy.[22−25]

Tumor acidic microenvironment (pH ∼6.0−7.0) is the most common property of solid tumors that has been widely utilized in nanotechnology to achieve targeting,[26] imaging,[27] drug control release,[28,29] and so on. Nam et al. introduced a 13 nm spherical gold nanoparticle that could exhibit pH-induced aggregation in mild acidic intracellular environments, and the aggregates of nanoparticles showed potential for photothermal cancer therapy. These results implied that the aggregation of nanospheres can be realized in a pH-induced manner, which in this work, was realized by the formation of mixed charged surfaces because of the hydrolysis of the surface ligands.[30] However, the pH-induced aggregation achieved by the breakage

Received: July 22, 2014
Accepted: October 6, 2014
Published: October 6, 2014

of chemical bond was lack of flexibility and the respond time was relatively long. The recent research[31,32] include ourselves indicated that the mixed-charge gold nanoparticles (MC-GNPs), with one of the counter charge ligands being weak electrolytic, also showed unique aggregation property under certain pH stimuli. The most exciting thing was that the pH at which the MC-GNPs aggregated could be regulated by changing the composition of the oppositely charged ligands on the surface.[32]

Size has always been considered as one of the most important fundamental properties of nanoparticles, which has great impacts on the physicochemical properties and biological behaviors of nanoparticles.[33−35] For spherical gold nanoparticles, increase in size slightly red-shifts the surface plasmon absorption maximum,[22] and aggregation from larger nanoparticles often results in red-shifts to much longer wavelength.[23] Therefore, the examination of the photothermal therapy capacity of the aggregates formed from different size nanoparticles can provide a better understanding of the way to improve the photothermal therapy efficacy. However, the current investigation in pH-induced aggregation behaviors of spherical MC-GNPs is mainly conducted on nanoparticles in relatively small sizes (≤16 nm). The preparation of pH sensitive MC-GNPs in larger size remains a big challenge because of their worse dispersive stability. Detailed studies on pH-induced aggregation behaviors of those large MC-GNPs are necessary, which may develop the understanding of realizing better photothermal performances using the MC-GNPs as photosentisizers.

In this paper, we prepared the MC-GNPs in four different sizes (15 nm, 21 nm, 33 and 53 nm) to explore the pH-induced aggregation achieved by the mixed-charge protecting strategy. All of the MC-GNPs were surface modified by the mixed-charge self-assembled monolayer with a mixture of a positively charged (10-mercaptodecyl) trimethylammonium bromide (TMA) and a negatively charged 11-mercaptoundecanoic acid (MUA). The pH-sensitive aggregation behaviors of the MC-GNPs were investigated by changing the proportion of surface counter charge ligands or the size of GNPs (Scheme 1). By virtue of the knowledge obtained from the above, four different size of the MC-GNPs that all responded to the tumor acidic pH were successfully prepared. Then the photothermal efficacy and ablation of cancer cells of these MC-GNPs in their aggregation state had been examined in vitro.

Scheme 1. Schematic Illustration of the MC-GNPs with Different pH-Induced Aggregation Behaviors Obtained by Adjusting the Counter Charge Ligands Feed Ratio and the Size of GNPs (Not to Scale)

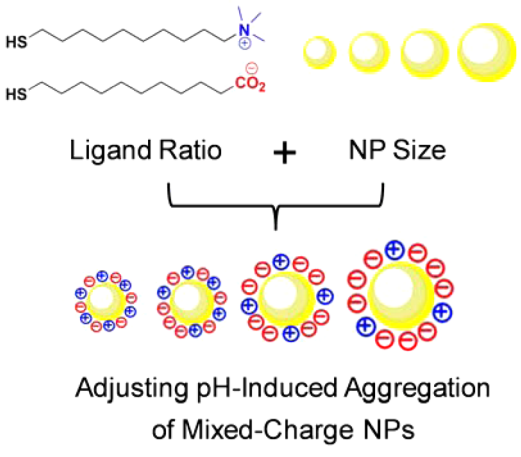

2. EXPERIMENTAL SECTION

Materials. The alkanethiol TMA with positively charged terminal group was synthesized according to the procedures described previously.[36] The alkanethiol MUA with negatively charged terminal group was purchased from J&K Chemical Ltd. (Shanghai, China). Hydrogen tetrachloroaurate hydrate ($HAuCl_4·4H_2O$), trisodium citrate dehydrate ($C_6H_5Na_3O_7·2H_2O$) and other chemicals and reagents were purchased from Sinopharm Chemical Reagent Co., Ltd. The HepG2 (liver hepatocellular carcinoma) cell line was purchased from China Center for Typical Culture Collection. All reagents were used without further purification

Synthesis of Gold Nanoparticles (GNPs) in Different Sizes. Spherical GNPs in different sizes were synthesized by using the standard citrate reduction method.[37] In this method, GNPs that differ in size can be prepared by adjusting the amount of added sodium citrate, which acts as the reducing agent. Briefly, 1.214 mL of 10 mM $HAuCl_4·4H_2O$ solution in 50 mL of Milli-Q water was heated to boil. With vigorous stirring, a certain amount of (1.5 mL, 1 mL, 0.75 and 0.5 mL were used to obtain different size GNPs, respectively) freshly prepared sodium citrate(1%,w/v) was added to the boiling solution. The mixing solution was kept boiling for another 30 min and was cooled to the room temperature.

Synthesis of the MC-GNPs in Different Sizes with the Same Ligand Feed Ratio. The ligand solution to modify the surface of GNPs was prepared by mixing the same volume of 20 mM MUA and 20 mM TMA solution together, and 0.625 mL of the ligand mixture solution was added to the ~50 mL citrate-coated GNP solution under vigorous stirring. The molar ratio between the total amount of those two ligands and the amount of Au atom was 2:1. The mixing solution was kept under stirring for 24 h and then was purified by centrifugation at 15 000 rpm for 15 min. The centrifugation procedure was conducted twice and then the precipitates were dissolved and dispersed in 2 mL of mili-Q water. Size and size distribution were determined from transmission electron microscopy (TEM) images (JEM-1230EX TEM, 80 kV, bright field mode) using the analysis software ImageJ (sample amount >150). The sizes of those four different GNPs were 15 ± 1.2 nm, 21 ± 4.1 nm, 33 ± 5.8 nm, and 53 ± 7.2 nm, respectively. Also, the dynamic light scattering (DLS) analysis (Zetasizer Nano-ZS from Malvern Instruments, 633 nm He−Ne laser, 25 °C with a detection angle of 173°) was used to determine the MC-GNPs hydrodynamic size. Here, we refer to the molar feed ratio between MUA and TMA as α.

Exploration of the Size Effect on the pH-Induced Aggregation Behaviors of the MC-GNPs (α = 1). Two methods were used to evaluate pH-induced aggregation behaviors of the MC-GNPs (α = 1) in different sizes. First, the pH-sensitive behaviors of the MC-GNPs were investigated by examining the stability of the MC-GNPs added in a series of 50 mM phosphate buffered (PB) solution that differed in pH values. The stability (dispersed or aggregated) of the MC-GNPs was confirmed by UV−vis spectra, as the aggregation of the MC-GNPs would result in red-shift in the absorption spectra. This method gave us a quick glimpse of the pH-induced aggregation behavior of the MC-GNPs. To further determine the exact pH transition point of the MC-GNPs, a chemical titration method was used.[32] That is, with the presence of a pH meter, the MC-GNPs solution was adjusted to pH 10 by 1 M sodium hydroxide, then was titrated by 1 M, 1 mM and 0.05 mM hydrochloric acid (using acid in proper concentration to minimize the increase of solution volume) to find out the abrupt transition point at which the MC-GNPs perform pH-induced aggregation behaviors. The solution was measured by UV−vis spectrometer (Shimadzu UV-2505) at certain pH intervals to determine the stability of the MC-GNPs solution more subtly and convincingly.

Tailoring pH-Sensitive Range of the MC-GNPs by Changing the Feed Ratio α of Ligands. The pH at which the well dispersed

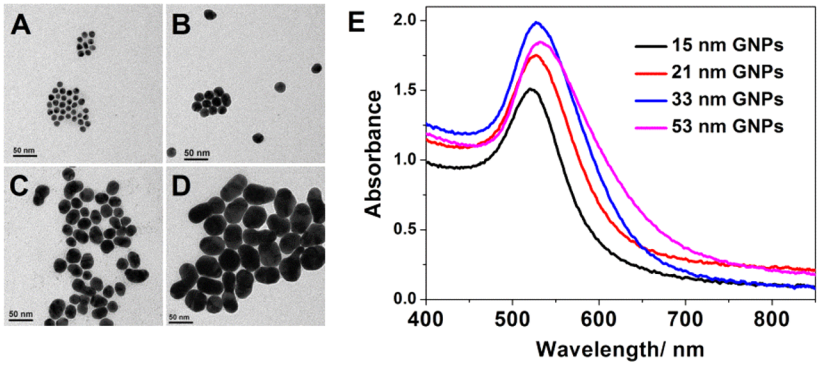

Figure 1. Representative TEM images of MC-GNPs with size of (A) 15, (B) 21, (C) 33, and (D) 53 nm, respectively. (E) UV−vis spectra of freshly prepared MC-GNPs.

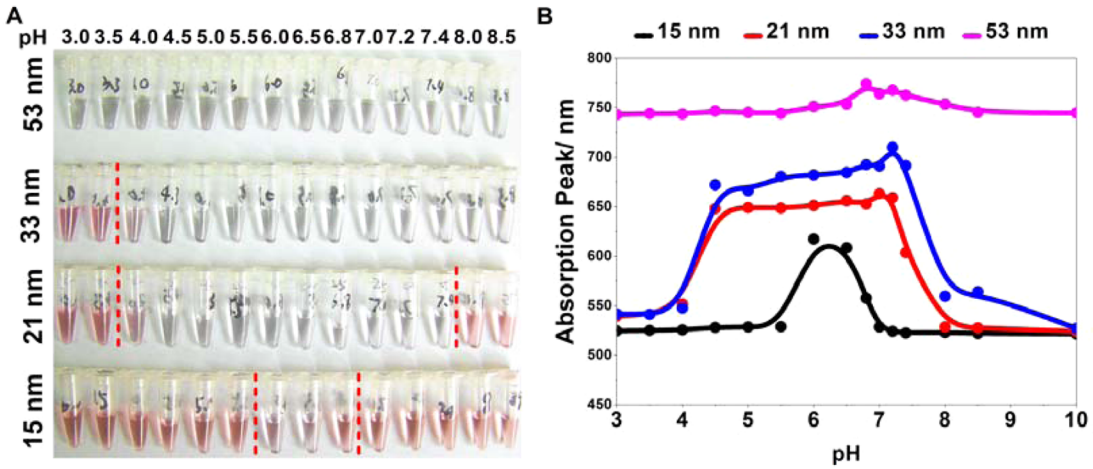

Figure 2. pH-induced aggregation behaviors of the MC-GNPs (α = 1) in different sizes. (A) Digital image of different size MC-GNPs incubated in 50 mM PB solution of different pH values. (B) Wavelength of the absorbance peak of different size MC-GNPs in PB solution detected by UV−vis spectrometer.

NPs formed aggregates was tuned by changing the feed ratio of the two counter charge ligands. Here, we increased the proportion of MUA in the total ligands amount, and a decrease in the MC-GNPs' aggregation pH value was observed. To obtain MC-GNPs in different sizes that respond to the tumor site acidic environment, we changed the value of α for several times. Since the 15 nm MC-GNPs (α = 1) already had the ability to respond to tumor acidic pH, the value of α was kept at 1 and acted as a control for the other size MC-GNPs. The sizes of the MC-GNPs aggregates were characterized by TEM and DLS.

NIR Photothermal Conversion Efficiency. The four different size MC-GNPs which were sensitive to the tumor acidic pH were added to pH 7.4 and pH 6.5 PB solution separately to make 1 mL 20 μg/mL solution. The temperature rise of each solution was recorded after 2 min irradiation by 13.8 W/cm^2 808 nm continuous wave (CW) laser (MDL-N-808 nm, Changchun New Industries Optoelectronics Tech. Co., Ltd., ~6 mm diameter spot-size). The pH 7.4 and pH 6.5 solution without MC-GNPs were used as a control. To examine the repeatability of photothermal conversion performances, the 53 nm MC-GNPs aggregated in 1 mL pH 6.5 PB solution was irradiated for 5 times and the temperature rise after each irradiation was recorded.

Photothermal Ablation of Cancer Cells. HepG2 cells were seeded at a density of 30 000 cells/well in 96-well plates and cultured with regular growth medium consisting of high-glucose DMEM (pH 7.4) for 24 h before experimentation. Then the medium was replaced with 40 μL 50 μg/mL MC-GNPs solution (added to pH 6.5 DMEM medium) of different sizes. The cell growth medium with either pH 7.4 or pH 6.5 was used as a control. The cells incubated with the different size MC-GNPs were irradiated by a 25.5 W/cm^2 808 nm NIR CW laser (Hi-Tech Optoelectronics Co., Ltd.) with a 1 mm focused spot size for 1 min. After irradiation, the MC-GNPs solution was replaced by pH 7.4 DMEM medium. The cells were stained with fluorescein diacetate (FDA) to determine the cell viability, as live cells could give out green fluorescence from FDA with the inside esterase, whereas dead cells could not give out fluorescence.

3. RESULTS AND DISCUSSION

pH-Induced Aggregation Behaviors of Different Size MC-GNPs with the Same Surface Ligand Composition. The four different size GNPs were surface modified with the MUA and TMA with the feed ratio α equals 1 (α refers to the molar ratio between MUA and TMA) according to the method reported before for preparing 16 nm MC-GNPs.[31] The sizes of the MC-GNPs measured by TEM were 15 ± 1.2, 21 ± 4.1, 33 ± 5.8, and 53 ± 7.2 nm, respectively (Figure 1). The DLS measurements showed the hydrodynamic size and size distribution of the MC-GNPs (See Figure S1 in the Supporting Information). The pH sensitivity of the MC-GNPs was examined by adding the MC-GNPs to PB solution of different pH values. Distinguished pH-induced aggregation behaviors among those four different size MC-GNPs (α = 1) could be roughly checked from the concomitant colorimetric change of the MC-GNPs solution (Figure 2A), as the well-dispersed MC-GNPs showed red wine color, whereas the aggregated MC-GNPs showed blue or purple color. Accurate pH sensitivity and the degree of aggregation were studied using UV−vis spectra of the MC-GNPs solution. Figure 2B showed the wavelengths of

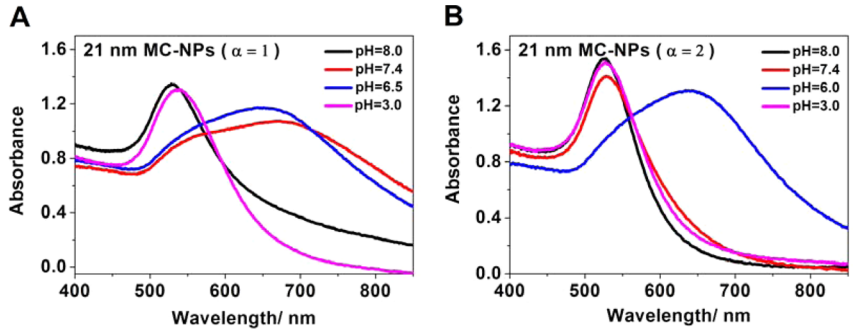

Figure 3. pH-induced aggregation behaviors can be tailored by changing the feed ratio α of the surface counter charge ligands. (A) 21 nm MC-GNPs with α = 1 aggregated at pH 7.4, whereas (B) 21 nm MC-GNPs α = 2 dispersed well at pH 7.4.

the light absorption peak of different size MC-GNPs (Detailed spectra of each size MC-GNPs were presented in Figure S2 in the Supporting Information) in PB solution at different pH. Consistent with the work reported before,[31] the smallest 15 nm MC-GNPs (α = 1) dispersed well in pH 7.4 phosphate buffer (PB, 50 mM) solution while aggregated in the PB solution at the tumor acidic pH 6.8. At certain pH range below the aggregation transition pH, the MC-GNPs still formed aggregates. When the pH of the MC-GNPs solution became rather acidic, such as pH 5.0, the MC-GNPs would be dispersed again and the absorption peak in UV−vis spectra returned to the well-dispersed state's position. Comparing the pH-induced aggregation behaviors among those different size MC-GNPs, an increasing trend in the aggregation transition pH values was observed as the size of the MC-GNPs increased, and so did the pH range in which the MC-GNPs formed aggregates. For the biggest 53 nm MC-GNPs, the MC-GNPs were no longer stable regardless of the pH of the solution and instability was also observed during the storage. More detailed observation of the pH-induced aggregation behaviors was conducted by chemical titration method (see Figure S3 in the Supporting Information) and the abrupt transition pH at which the MC-GNPs performed pH-induced aggregation behaviors were obtained, that is pH 7.0, 7.8, and 9.2 for the 15, 21, and 33 nm MC-GNPs, respectively. The 53 nm MC-GNPs did not exhibit abrupt pH-induced transition within the whole tested pH range, for the GNPs could not be stabilized by the ligands modification of α = 1.

The aggregation of MC-GNPs was mainly caused by the disturbance of the balance of the interparticle interaction. There was a competition in the interparticle interaction among the attractive electrostatic interaction, hydrogen-bonding interaction, van der Waals interaction and repulsive hydration interaction, electrostatic interaction and other interactions.[38,39] The amount of the negative charges on the MC-GNPs surface varied as the pH of the solution changed, because some of the negative charge would be shielded because of the protonation of the carboxyl group in MUA at lower pH, which affected the interparticle interaction and in some certain cases would result in the aggregation of the MC-GNPs. In the solution with relatively high or low pH, the NPs surface would be dominated either by negative or positive charge, and the MC-GNPs were stable owing to the strong electrostatic repulsion. The different size MC-GNPs with the same feed ratio=1 showed diverse pH-sensitivity, which may be caused by the varied need for repulsive forces to stabilize the MC-GNPs in different sizes. At the same environmental pH, the repulsive interaction provided by the same ligand composition may be able to stabilize those small MC-GNPs but is not strong enough to keep the large-sized MC-GNPs dispersed, which endowed the large MC-GNPs with higher transition pH than the small ones with α = 1.

Those MC-GNPs (α = 1) in different sizes not only differed in the pH-induced aggregation behavior, but had distinguished red-shift performances (Figure 2B). In the dispersed states of the different size MC-GNPs, there was only a slight difference in the wavelength of absorption peak (Figure 1E). But when they formed aggregates, the degree of the red-shifts varied significantly. The MC-GNPs that bigger in size would red-shift to a longer wavelength after aggregation. For now, the NIR laser commonly used in phothothemal therapy are of 808 nm wavelength.[40] Hence, efficient aggregation-induced enhancement of the light absorption around 800 nm is in great help for increasing the generated heat energy through photothermal conversion, since larger amount of light is ready to be converted into heat. As to large MC-GNPs such as 33 or 53 nm, the aggregation of the MC-GNPs shifted the light absorption to comparable long wavelength and had considerable absorption near the 800 nm wavelengths, which held great promise in photothermal cancer therapy.

With the same ligand feed ratio α = 1, the MC-GNPs in different sizes showed diverse pH-induced aggregation behaviors, but only those MC-GNPs with the size of 15 nm exhibited effective pH-sensitivity to the tumor acidic pH. The ideal photothermal therapy based on MC-GNPs is that the MC-GNPs are well-dispersed at the normal tissue pH 7.4 while exhibit a pH-induced aggregation in respond to the tumor site acidic pH 6.8−6.5. And the aggregation of the MC-GNPs should result in efficient red-shifts so that considerable enhancement in the NIR light absorption can be achieved, which means after the NIR light irradiation enough heat can be generated to kill cancer cells. Hence, further tailoring of surface ligands composition was required to obtain MC-GNPs that could aggregate abruptly at pH 7.0 to pH 6.5.

Tailoring the pH-Induced Aggregation Behaviors of the MC-GNPs by Changing the Counter Charge Ligands Feed Ratio α. By raising the feed ratio α, a decrease in aggregation transition pH was observed in the MC-GNPs. For example (Figure 3), after raising the feed ratio α of the 21 nm MC-GNPs from 1 to 2, the NPs showed very different aggregation behaviors than before. The 21 nm MC-GNPs with α = 1 aggregated at pH 7.4, whereas the 21 nm MC-GNPs at α = 2 were well dispersed at pH 7.4. This meant that by increasing the MUA proportion in the feed ligands, the MC-GNPs could show a decrease in aggregation pH. So it could be utilized to lower the pH at which the MC-GNPs aggregated by increasing the proportion of the pH-sensitive weak electrolyte

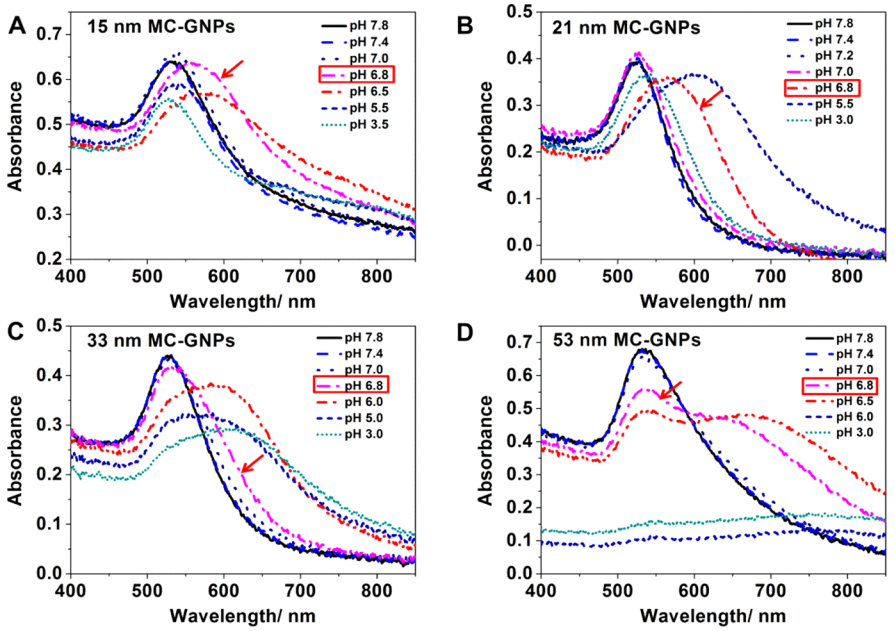

Figure 4. Precise aggregation transition pH values of (A) 15, (B) 21, (C) 33, and (D) 53 nm MC-GNPs which responded to the tumor acidic environment. The pH at which the MC-GNPs started to form aggregates was pointed out and only partial of the UV-vis spectra were presented for simplicity.

ligand MUA. As discussed before, the aggregation behaviors of the MC-GNPs would be affected significantly by the change in the amount of negative charge on the NPs' surface, since the amount of positive charge from the TMA ligand remained the same no matter what pH the solution was. So increasing the proportion of the MUA in the feed ligands would lead the MC-GNPs to aggregate at lower pH, for more H^+ ions are needed to protonize the negatively charged MUA ligands so that the aggregation could happen.

With a series of regulation of the surface ligands composition, diverse pH-induced aggregation behaviors of the MC-GNPs in different sizes were observed (see Figure S4 in the Supporting Information), and the size effect in the red-shift ability after aggregation remained the same as before. The results implied that by tailoring the surface ligand composition, MC-GNPs with various pH-induced aggregation behaviors can be obtained. Most inspiringly, MC-GNPs in four different sizes that all exhibited desired pH-induced aggregation at the tumor acidic pH were successfully prepared by virtue of the knowledge obtained above. Those MC-GNPs were 15 nm MC-GNPs with α = 1, 21 nm MC-GNPs with α = 2, 33 nm MC-GNPs with α = 4, and 53 nm MC-GNPs with α = 4. The precise aggregation transition pH was determined by the chemical titration method for the MC-GNPs in different sizes (Figure 4).

Photothermal Therapy Efficacy of the MC-GNPs in Different Sizes. The four different size MC-GNPs with the ability to exhibit aggregation behaviors in response to tumor site acidic pH were obtained simply by tailoring the feed ratio of the surface counter charge ligands. Panels A and B in Figure 5 showed the light absorption performances of the four different size MC-GNPs in dispersed state and aggregated state. All of the MC-GNPs exhibited red-shifts in their light absorption spectra when they formed aggregates and an increasing trend in the degree of red-shifts was observed as the size of the MC-GNPs increased, which was in agreement with the previous results. Then those four different size MC-GNPs that all went through the pH-induced aggregation at tumor acidic pH were used to explore the photothermal therapy efficacy of MC-GNPs.

Plasmon-enabled photothermal conversion efficiency of those four different size MC-GNPs was evaluated by measuring the temperature rise of the MC-GNPs solution after irradiation by the NIR continuous wave (CW) laser. The MC-GNPs in four different sizes were added to pH 7.4 and pH 6.5 PB solutions respectively, and the temperature rise of the MC-GNPs solutions after the NIR light irradiation was recorded (Figure 5C). A significant difference in temperature rise between the dispersed state at pH 7.4 and the aggregated state at pH 6.5 for each size MC-GNPs was observed, which suggested that the aggregation of the MC-GNPs indeed improved the photothermal conversion efficiency. Moreover, an increase in temperature rise was observed when the original size of the MC-GNPs to form aggregates increased. It was because more NIR light could be absorbed by the aggregates of large size MC-GNPs as Figure 5B showed, and hence more heat would be generated through plasmon-enabled conversion after the NIR laser irradiation. What's more, the repeatability of photothermal conversion ability was examined by irradiating the MC-GNPs (53 nm in size) for five times. Figure 5D showed the temperature of the MC-GNPs solution through the five time irradiation. No significant difference could be told from the temperature rise degrees of the MC-GNPs aggregates solution during the five time irradiation, which suggested the aggregates of the MC-GNPs were quite stable under reasonable power of laser irradiation.

Cell ablation efficacy that achieved by the MC-GNPs was evaluated on the HepG2 cancer cells. The aggregates of different size MC-GNPs formed in the pH 6.5 cell growth media DMEM were added to the HepG2 cells, then were irradiated by the NIR CW laser. The cells were then stained by FDA. The live cells and dead cells could be told from the fluorescence under fluoresce microscope as live cells could give out a green fluorescence while no fluorescence could be

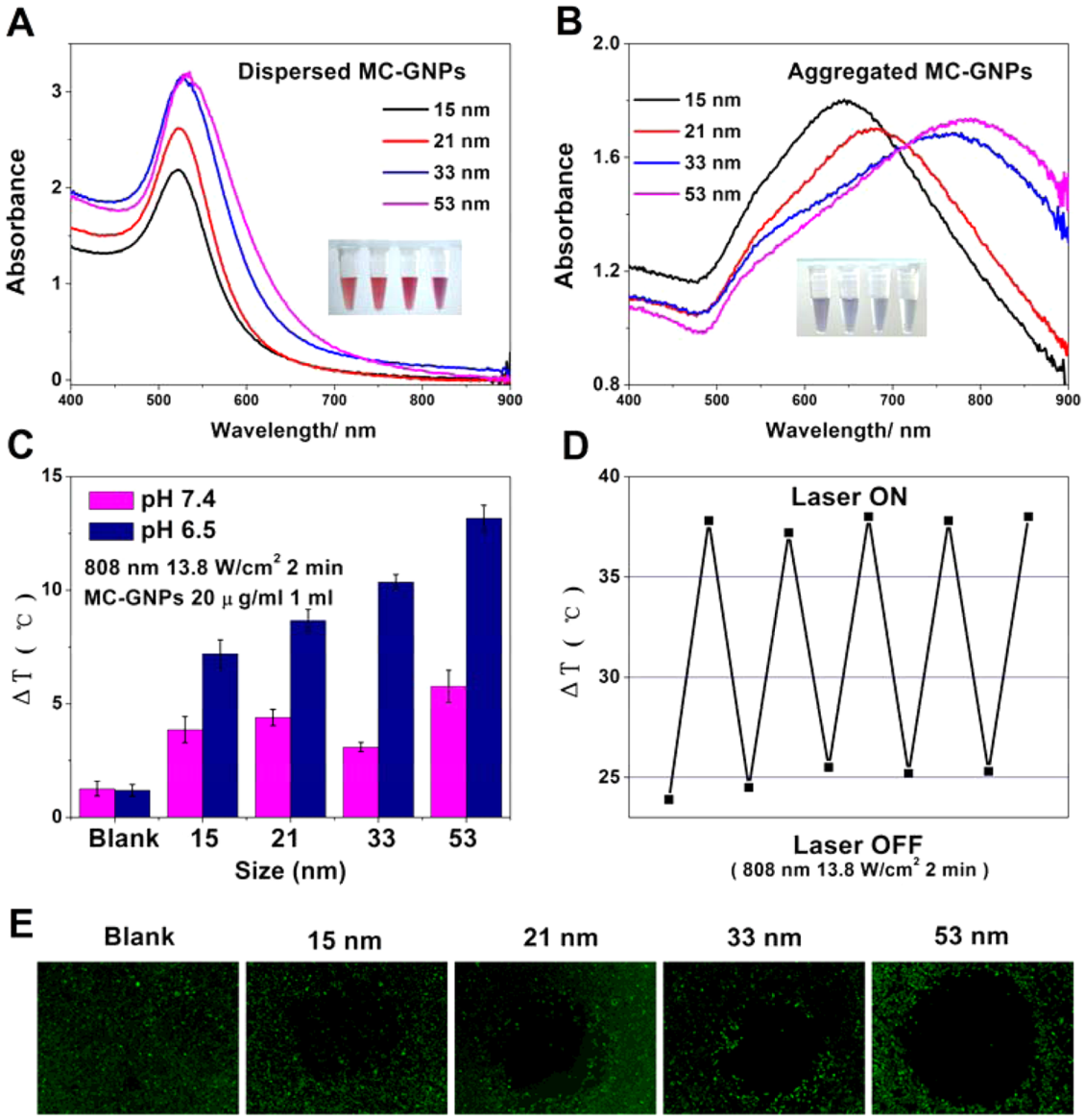

Figure 5. Photothermal therapy efficacy of tumor acidic pH sensitive MC-GNPs. (A) Dispersed and (B) aggregated state of MC-GNPs. (Insets are the images of the MC-GNPs solutions at corresponding pH. From left to right are 15, 21, 33, and 53 nm MC-GNPs, respectively). (C) Photothermal conversion performances of the MC-GNPs after the NIR CW light irradiation. (D) Temperature of the 53 nm MC-GNPs solution during 5 times NIR irradiation. (E) Ablation of HepG2 cells with MC-GNPs in different sizes after the NIR light irradiation. Cells were stained with FDA, thus live cells could give out green fluorescence while dead cells could not.

observed in dead cells. As Figure 5E showed, the HepG2 cells with the aggregates of the MC-GNPs could be killed to some extent after the NIR light irradiation. The ablation of the HepG2 cancer cells were intensified in those cells with the MC-GNPs aggregates formed from large size MC-GNPs. Among others, the largest 53 nm MC-GNPs showed the best photothermal therapy efficacy, which was well consistent with the photothermal conversion efficiency mentioned before. No significant toxicity of the different size MC-GNPs to the HepG2 cells was observed.

To further investigate the influence of the size of the MC-GNPs aggregates on the photothermal efficacy, we added MC-GNPs in the four different sizes that all responded to the tumor site pH into pH 6.5 cell growth medium separately. The aggregation behaviors were observed by TEM and DLS. The TEM images of the aggregates formed from four different size MC-GNPs and their size and size distribution are shown in Figure 6. No dramatic size difference was observed among the aggregates of the 21, 33, and 53 nm MC-GNPs while their photothermal efficacy varied significantly, which meant the photothermal efficacy did not depend on the size of the formed MC-GNPs aggregates, but heavily influenced by the original size of the MC-GNPs. This was because the light absorption ability was different among those MC-GNPs aggregates formed from different size, so was the heat generated by the aggregates. Moreover, the aggregation of the different size MC-GNPs for cell endocytosis would merit further investigation.[41]

In this study, it was suggested that the mixed-charge strategy was ready to endow NPs with controllable pH-sensitivity, and the pH-induced aggregation behaviors were able to be tailored by changing the size or the composition of the two opposite ligands on NPs surface. The MC-GNPs with desired sensitivity to the tumor site acidic pH, showed encouraging photothermal cancer therapy potential, especially those large in size. To

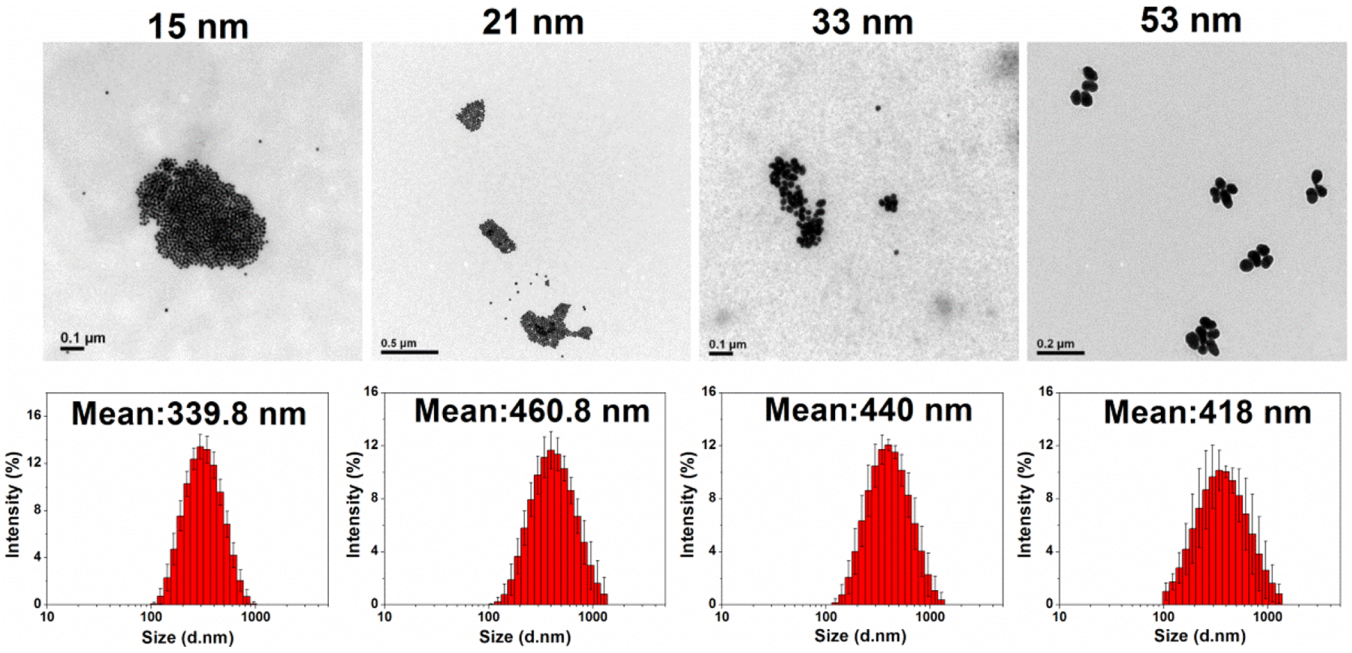

Figure 6. Aggregates formed from different size MC-GNPs. The TEM images were displayed on the upper row and below each TEM image was the corresponding hydrodynamic size and size distribution characterized by DLS.

further develop the MC-GNPs system, specific ligands with functionality could be introduced to the NPs' surface to obtain multifunctional nanomaterials.

4. CONCLUSIONS

In summary, we demonstrated here that the mix-charged self-assembled monolayers can serve as a facile method to prepare large gold nanoparticles with tunable pH-induced aggregation behaviors. The basic law of the pH-induced aggregation of the MC-GNPs influenced by surface charge composition and size factors was systematically investigated. The results indicated that by increasing the negatively charged ligands proportion or decreasing the MC-GNPs size, the aggregation transition pH of the MC-GNPs would decrease, whose converse is also true. Given this, four different size MC-GNPs with desired tumor acidic pH induced aggregation were prepared. The photothermal efficacy had an increasing trend as the size of the MC-GNPs increased, and when it came to those 53 nm ones, the most encouraging photothermal therapy efficacy with HepG2 cancer cells was achieved. The mixed-charge self-assembly monolayers of the positively and negatively charged thiol ligands were then proved as an effective method to design pH sensitive large gold nanoparticles for better NIR photothermal cancer therapy.

■ ASSOCIATED CONTENT

Supporting Information

Additional figures showing size and size distribution of the different size MC-GNPs, UV−vis spectra of the different size MC-GNPs with α = 1and their abrupt transition pH measured by chemical titration method, detailed information about tailoring the pH-induced aggregation behaviors by changing the ligand feed ratio α, and the HepG2 cells without any NIR irradiation indicating no significant toxicity of the MC-GNPs. This material is available free of charge via the Internet at http://pubs.acs.org.

■ AUTHOR INFORMATION

Corresponding Author

*E-mail: jijian@zju.edu.cn.

Author Contributions

†H.L. and X.L. contributed equally.

Notes

The authors declare no competing financial interest.

■ ACKNOWLEDGMENTS

Financial support from the National Science Fund for Distinguished Young Scholars (51025312), the National Basic Research Program of China (2011CB606203), NSFC-50830106 and 21174126, Open Project of State Key Laboratory of Supramolecular Structure and Materials (SKLSSM 201204), and Research Fund for the Doctoral Program of Higher Education of China (20110101110037, 20110101120049, and 20120101130013) is gratefully acknowledged. We thank Ying Xu and Hua Wang for TEM.

■ ABBREVIATIONS

NIR;near-infrared

MC-GNPs;mixed-charge gold nanoparticles

■ REFERENCES

(1) Helmchen, F.; Denk, W. Deep Tissue Two-Photon Microscopy. *Nat. Methods.* **2005**, *2*, 932−940.

(2) Kennedy, L. C.; Bickford, L. R.; Lewinski, N. A.; Coughlin, A. J.; Hu, Y.; Day, E. S.; West, J. L.; Drezek, R. A. A New Era for Cancer Treatment: Gold-Nanoparticle-Mediated Thermal Therapies. *Small* **2011**, *7*, 169−183.

(3) Cheng, L.; Yang, K.; Chen, Q.; Liu, Z. Organic Stealth Nanoparticles for Highly Effective in Vivo Near-Infrared Photothermal Therapy of Cancer. *ACS Nano* **2012**, *6*, 5605−5613.

(4) Song, C. W.; Park, H. J.; Lee, C. K.; Griffin, R. Implications of Increased Tumor Blood Flow and Oxygenation Caused by Mild Temperature Hyperthermia in Tumor Treatment. *Int. J. Hyperth.* **2005**, *21*, 761−767.

(5) Li, J. L.; Day, D.; Gu, M. Ultra-Low Energy Threshold for Cancer Photothermal Therapy Using Transferrin-Conjugated Gold Nanorods. *Adv. Mater.* **2008**, *20*, 3866−3871.
(6) Guo, R.; Zhang, L.; Qian, H.; Li, R.; Jiang, X.; Liu, B. Multifunctional Nanocarriers for Cell Imaging, Drug Delivery, and Near-IR Photothermal Therapy. *Langmuir* **2010**, *26*, 5428−5434.
(7) Ren, F.; Bhana, S.; Norman, D. D.; Johnson, J.; Xu, L.; Baker, D. L.; Parrill, A. L.; Huang, X. Gold Nanorods Carrying Paclitaxel for Photothermal-Chemotherapy of Cancer. *Bioconjugate Chem.* **2013**, *24*, 376−386.
(8) Chen, J.; Wang, D.; Xi, J.; Au, L.; Siekkinen, A.; Warsen, A.; Li, Z.-Y.; Zhang, H.; Xia, Y.; Li, X. Immuno Gold Nanocages with Tailored Optical Properties for Targeted Photothermal Destruction of Cancer Cells. *Nano Lett.* **2007**, *7*, 1318−1322.
(9) Au, L.; Zheng, D.; Zhou, F.; Li, Z.-Y.; Li, X.; Xia, Y. A Quantitative Study on the Photothermal Effect of Immuno Gold Nanocages Targeted to Breast Cancer Cells. *ACS Nano* **2008**, *2*, 1645−1652.
(10) Gao, L.; Fei, J.; Zhao, J.; Li, H.; Cui, Y.; Li, J. Hypocrellin-Loaded Gold Nanocages with High Two-Photon Efficiency for Photothermal/Photodynamic Cancer Therapy in Vitro. *ACS Nano* **2012**, *6*, 8030−8040.
(11) Kim, J.; Park, S.; Lee, J. E.; Jin, S. M.; Lee, J. H.; Lee, I. S.; Yang, I.; Kim, J.-S.; Kim, S. K.; Cho, M.-H.; Hyeon, T. Designed Fabrication of Multifunctional Magnetic Gold Nanoshells and Their Application to Magnetic Resonance Imaging and Photothermal Therapy. *Angew. Chem.* **2006**, *118*, 7918−7922.
(12) Vankayala, R.; Lin, C.-C.; Kalluru, P.; Chiang, C.-S.; Hwang, K. C. Gold Nanoshells-Mediated Bimodal Photodynamic and Photothermal Cancer Treatment Using Ultra-Low Doses of Near Infra-Red Light. *Biomaterials* **2014**, *35*, 5527−5538.
(13) Wang, Y.; Black, K. C. L.; Luehmann, H.; Li, W.; Zhang, Y.; Cai, X.; Wan, D.; Liu, S.-Y.; Li, M.; Kim, P.; Li, Z.-Y.; Wang, L. V.; Liu, Y.; Xia, Y. Comparison Study of Gold Nanohexapods, Nanorods, and Nanocages for Photothermal Cancer Treatment. *ACS Nano* **2013**, *7*, 2068−2077.
(14) Rivera Gil, P.; Hühn, D.; del Mercato, L. L.; Sasse, D.; Parak, W. J. Nanopharmacy: Inorganic Nanoscale Devices as Vectors and Active Compounds. *Pharmacol. Res.* **2010**, *62*, 115−125.
(15) Huang, X.; El-Sayed, I. H.; Qian, W.; El-Sayed, M. A. Cancer Cell Imaging and Photothermal Therapy in the Near-Infrared Region by Using Gold Nanorods. *J. Am. Chem. Soc.* **2006**, *128*, 2115−2120.
(16) Wang, J.; Zhu, G.; You, M.; Song, E.; Shukoor, M. I.; Zhang, K.; Altman, M. B.; Chen, Y.; Zhu, Z.; Huang, C. Z.; Tan, W. Assembly of Aptamer Switch Probes and Photosensitizer on Gold Nanorods for Targeted Photothermal and Photodynamic Cancer Therapy. *ACS Nano* **2012**, *6*, 5070−5077.
(17) Dickerson, E. B.; Dreaden, E. C.; Huang, X.; El-Sayed, I. H.; Chu, H.; Pushpanketh, S.; McDonald, J. F.; El-Sayed, M. A. Gold Nanorod Assisted Near-Infrared Plasmonic Photothermal Therapy (PPTT) of Squamous Cell Carcinoma in Mice. *Cancer Lett.* **2008**, *269*, 57−66.
(18) Choi, W. I.; Kim, J.-Y.; Kang, C.; Byeon, C. C.; Kim, Y. H.; Tae, G. Tumor Regression In Vivo by Photothermal Therapy Based on Gold-Nanorod-Loaded, Functional Nanocarriers. *ACS Nano* **2011**, *5*, 1995−2003.
(19) Okuno, T.; Kato, S.; Hatakeyama, Y.; Okajima, J.; Maruyama, S.; Sakamoto, M.; Mori, S.; Kodama, T. Photothermal Therapy of Tumors in Lymph Nodes Using Gold Nanorods and Near-Infrared Laser Light. *J. Controlled Release* **2013**, *172*, 879−884.
(20) Wang, S.; Lu, W.; Tovmachenko, O.; Rai, U. S.; Yu, H.; Ray, P. C. Challenge in Understanding Size and Shape Dependent Toxicity of Gold Nanomaterials in Human Skin Keratinocytes. *Chem. Phys. Lett.* **2008**, *463*, 145−149.
(21) Aillon, K. L.; Xie, Y.; El-Gendy, N.; Berkland, C. J.; Forrest, M. L. Effects of Nanomaterial Physicochemical Properties on in vivo Toxicity. *Adv. Drug Delivery Rev.* **2009**, *61*, 457−466.
(22) Huang, X.; Jain, P. K.; El-Sayed, I. H.; El-Sayed, M. A. Plasmonic Photothermal Therapy (PPTT) Using Gold Nanoparticles. *Laser. Med. Sci.* **2008**, *23*, 217−228.
(23) Khlebtsov, B.; Zharov, V.; Melnikov, A.; Tuchin, V.; Khlebtsov, N. Optical Amplification of Photothermal Therapy with Gold Nanoparticles and Nanoclusters. *Nanotechnology* **2006**, *17*, 5167−5179.
(24) Huang, X.; Qian, W.; El-Sayed, I. H.; El-Sayed, M. A. The Potential Use of the Enhanced Nonlinear Properties of Gold Nanospheres in Photothermal Cancer Therapy. *Laser. Surg. Med.* **2007**, *39*, 747−753.
(25) Zharov, V. P.; Galitovskaya, E. N.; Johnson, C.; Kelly, T. Synergistic Enhancement of Selective Nanophotothermolysis with Gold Nanoclusters: Potential for Cancer Therapy. *Laser. Surg. Med.* **2005**, *37*, 219−226.
(26) Lee, E. S.; Gao, Z.; Bae, Y. H. Recent Progress in Tumor pH Targeting Nanotechnology. *J. Controlled Release* **2008**, *132*, 164−170.
(27) Li, C.; Xia, J.; Wei, X.; Yan, H.; Si, Z.; Ju, S. pH-Activated Near-Infrared Fluorescence Nanoprobe Imaging Tumors by Sensing the Acidic Microenvironment. *Adv. Funct. Mater.* **2010**, *20*, 2222−2230.
(28) Gao, G. H.; Li, Y.; Lee, D. S. Environmental pH-Sensitive Polymeric Micelles for Cancer Diagnosis and Targeted Therapy. *J. Controlled Release* **2013**, *169*, 180−184.
(29) Lee, E. S.; Na, K.; Bae, Y. H. Polymeric Micelle for Tumor pH and Folate-Mediated Targeting. *J. Controlled Release* **2003**, *91*, 103−113.
(30) Nam, J.; Won, N.; Jin, H.; Chung, H.; Kim, S. pH-Induced Aggregation of Gold Nanoparticles for Photothermal Cancer Therapy. *J. Am. Chem. Soc.* **2009**, *131*, 13639−13645.
(31) Liu, X.; Chen, Y.; Li, H.; Huang, N.; Jin, Q.; Ren, K.; Ji, J. Enhanced Retention and Cellular Uptake of Nanoparticles in Tumors by Controlling Their Aggregation Behavior. *ACS Nano* **2013**, *7*, 6244−6257.
(32) Pillai, P. P.; Huda, S.; Kowalczyk, B.; Grzybowski, B. A. Controlled pH Stability and Adjustable Cellular Uptake of Mixed-Charge Nanoparticles. *J. Am. Chem. Soc.* **2013**, *135*, 6392−6395.
(33) Petros, R. A.; DeSimone, J. M. Strategies in The Design of Nanoparticles for Therapeutic Applications. *Nat. Rev. Drug Discovery* **2010**, *9*, 615−627.
(34) Walkey, C. D.; Olsen, J. B.; Guo, H.; Emili, A.; Chan, W. C. W. Nanoparticle Size and Surface Chemistry Determine Serum Protein Adsorption and Macrophage Uptake. *J. Am. Chem. Soc.* **2011**, *134*, 2139−2147.
(35) Albanese, A.; Tang, P. S.; Chan, W. C. W. The Effect of Nanoparticle Size, Shape, and Surface Chemistry on Biological Systems. *Annu. Rev. Biomed. Eng.* **2012**, *14*, 1−16.
(36) Liu, X.; Huang, H.; Jin, Q.; Ji, J. Mixed Charged Zwitterionic Self-Assembled Monolayers as a Facile Way to Stabilize Large Gold Nanoparticles. *Langmuir* **2011**, *27*, 5242−5251.
(37) Frens, G. Controlled Nucleation for the Regulation of the Particle Size in Monodisperse Gold Suspensions. *Nature* **1973**, *241*, 20−22.
(38) Yang, H.; Heng, X.; Hu, J. Salt- and pH-Resistant Gold Nanoparticles Decorated with Mixed-Charge Zwitterionic Ligands, and Their pH-Induced Concentration Behavior. *Rsc Adv.* **2012**, *2*, 12648−12651.
(39) Yang, H.; Heng, X.; Wang, W.; Hu, J.; Xu, W. Salt-Induced Size-Selective Separation, Concentration, and Preservation of Zwitterion-Modified Gold Nanoparticles. *RSC Adv.* **2012**, *2*, 2671−2674.
(40) Zhang, Z.; Wang, J.; Chen, C. Gold Nanorods Based Platforms for Light-Mediated Theranostics. *Theranostics* **2013**, *3*, 223.
(41) Albanese, A.; Chan, W. C. Effect of Gold Nanoparticle Aggregation on Cell Uptake and Toxicity. *ACS Nano* **2011**, *5*, 5478−5489.